(3)

AMERICAN SOCIETY FOR METALS
Metals Park, Ohio 44073

Metals/Materials Technology Series

STRUCTURE PROPERTY RELATIONSHIPS IN A 25-Cr-7Ni-2Mo DUPLEX STAINLESS STEEL CASTING ALLOY

J. Chance, W. Coop, K. J. Gradwell
Mather & Platt Ltd., Rotating Machinery Division

C. V. Roscoe
Dept. of Metallurgy
University of Manchester, England

1982 ASM Metals Congress
St. Louis, Missouri
23–28 October 1982

8201-019

SAN: 204-7586

STRUCTURE PROPERTY RELATIONSHIPS IN A 25-Cr-7Ni-2Mo DUPLEX STAINLESS STEEL CASTING ALLOY

J. Chance, W. Coop, K.J. Gradwell
Mather & Platt Ltd., Rotating Machinery Division
C.V. Roscoe, Dept. of Metallurgy
University of Manchester, England

Metallographic and isothermal heat treatment techniques have been used to study the decomposition of ferrite into austenite and various other phases in a 25% Chromium, 7% Nickel, 2% Molybdenum duplex structured stainless steel casting alloy. The role of the various phase transformations in respect of their effect on the production of large thick section castings is discussed. The effect of nitrogen in respect of localised corrosion performance is assessed using cyclic anodic polarisation scans. C.O.D. measurements have been utilised to examine the use of intermediate temperature treatments to relieve stresses in general and to improve the toughness of weld deposits.

1.0 INTRODUCTION

In recent years duplex stainless steels and in particular the austenitic-ferritic grades have become increasingly popular for seawater and other arduous environments because of their good resistance to localised corrosion and near immunity to stress corrosion cracking. It is intended to show how the compositions of the 25Cr-5Ni family of alloys can be adjusted to suit the process demands of manufacture, and optimise the mechanical and corrosion resistant properties by microstructural control. Several papers do exist for background reading as an introduction to the austenitic-ferritic duplex stainless steels (1-3).

2.0 COMPOSITION

The base duplex alloy, Zeron 25 (a), used for all development studies was of the following wt-% composition.

Table 1

C	Mn	Si	Cr	Ni	Mo	N2
.04	.54	.57	24.4	5.6	2.5	0.12

Typical room temperature mechanical properties for the alloy in the solution treated and water quenched condition are shown in Table 2.

Table 2

0.2% Proof Stress MPa	U.T.S. MPa	Elong %	Impact Joules
480	685	29	100 (Charpy-V)

Typical corrosion performance data measured in terms of critical pitting and crevicing temperatures in artificial seawater using cyclic anodic polarisation scans are presented below.

Critical Pitting Temperature $49^{o}C$

Critical Crevicing Temperature $30^{o}C$

(a) Zeron 25 is a Registered Trademark of Mather & Platt Limited.

3.0 MICROSTRUCTURE

A typical duplex microstructure, shown in Figure 1, consists of 60-70% ferrite with widmanstätten austenite developed along grain boundaries and within the grains.

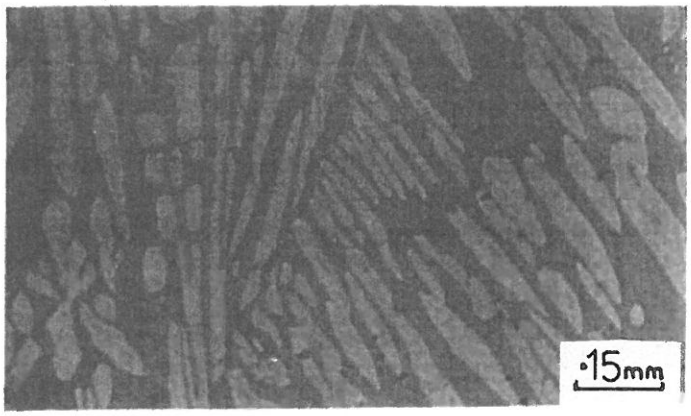

Figure 1. Duplex Microstructure of 25Cr-5Ni-2Mo alloy, as cast.

Discrete areas of fine secondary austenite develop after solution heat treatment.

The development of austenite from ferrite can best be studied by taking the alloy into a fully ferritic phase field and observing austenite formation in both isothermally heat treated and continuously cooled specimens. Figure 2 shows the microstructures from (a) a specimen held in the ferritic phase region for one hour and quenched, and (b) and (c) two specimens ferritised and isothermally transformed at 950°C, showing austenite developing with time. Unlike Southwick and Honeycombe (4) it was found impossible, on quenching, to retain a wholly ferritic matrix regardless of the solution treatment conditions employed. On quenching from 1310°C into iced brine the formation of a fine precipitate was unavoidable. Extraction replicas of these precipitates, Figure 3, have been analysed using a microprobe analyser which yielded a spectrum rich in chromium with small amounts of molybdenum, iron and manganése. Energy loss spectroscopy gave absorption edges for carbon and in some specimens, nitrogen. Analysis of diffraction patterns has given ambiguous results and the crystal structure of this chromium carbide/carbo-nitride may be $M_{23}C_6$ or, an as yet, unreported type.

Isothermal transformation experiments have been carried out in the temperature range 400-950°C and the phase transformation data is reported in Figure 4, together with results from other works (4-6). In addition to the two major phases of ferrite and austenite several additional phases occur during ageing, namely M_7C_3, $M_{23}C_6$, Sigma (σ), Chi, Laves, a martensitic austenite, γ_2 and a chromium solid solution precipitate, α'. However, only those phases that lie close to the left hand side of the time scale are of importance to a casting manufacturer, and thus discussion is limited to formation of γ_2, $M_{23}C_6$, σ and α'.

Figure 2: Development of austenite at 950°C

(a) 1 hour at 1310°C (b) 2 mins at 950°C (c) 1 hr 950°C

(a)

(b)

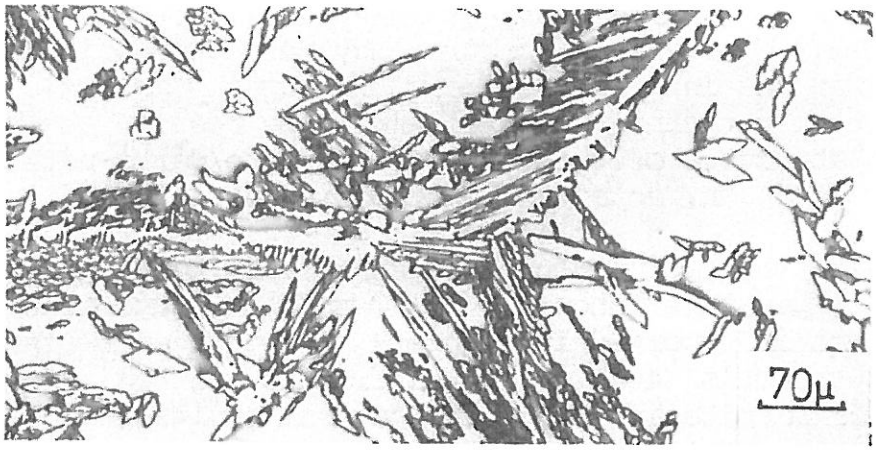

(c)

Figure 3 (a) Extraction replica of precipitates formed during the quench from ferritisation temperature of 1400°C

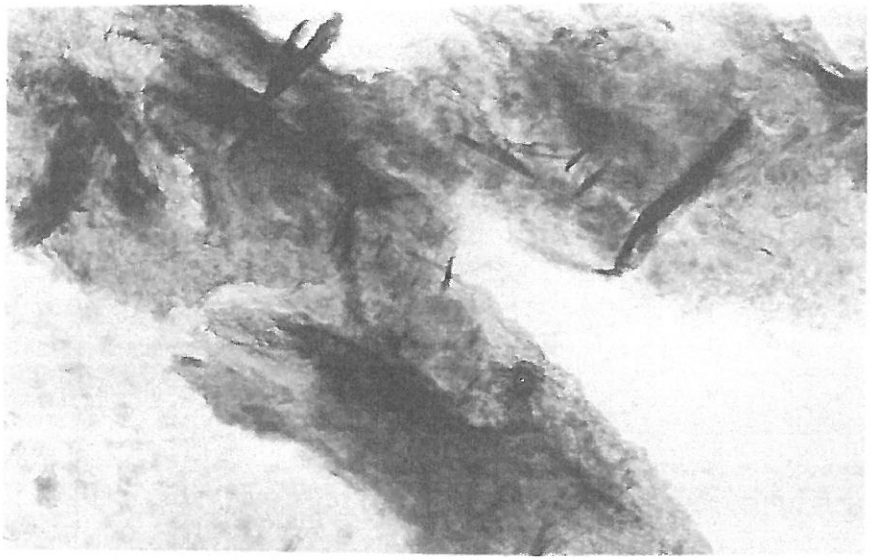

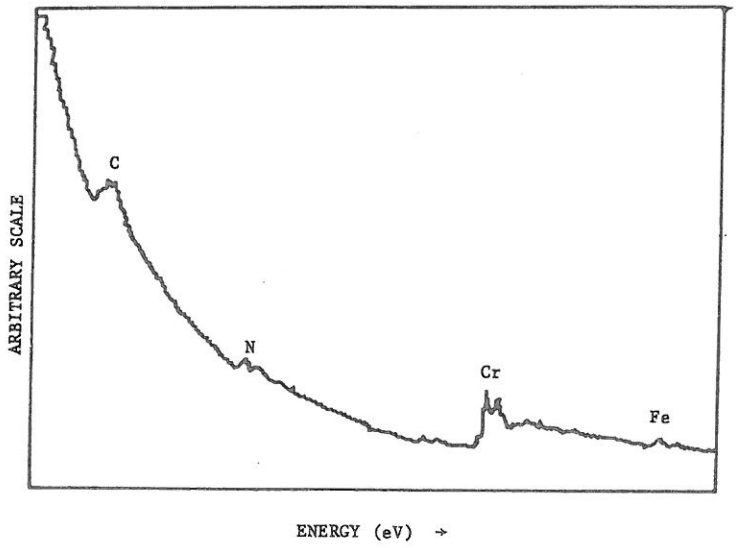

(b) Energy loss data showing carbon and nitrogen absorption edges

(c) Wt % Composition from energy dispersive analysis

Si	Mo	Cr	Mn	Fe	Ni
3.16	10.08	69.18	3.80	12.11	1.66
±.58	±1.49	± 2.74	± 0.61	± 1.17	± 0.38

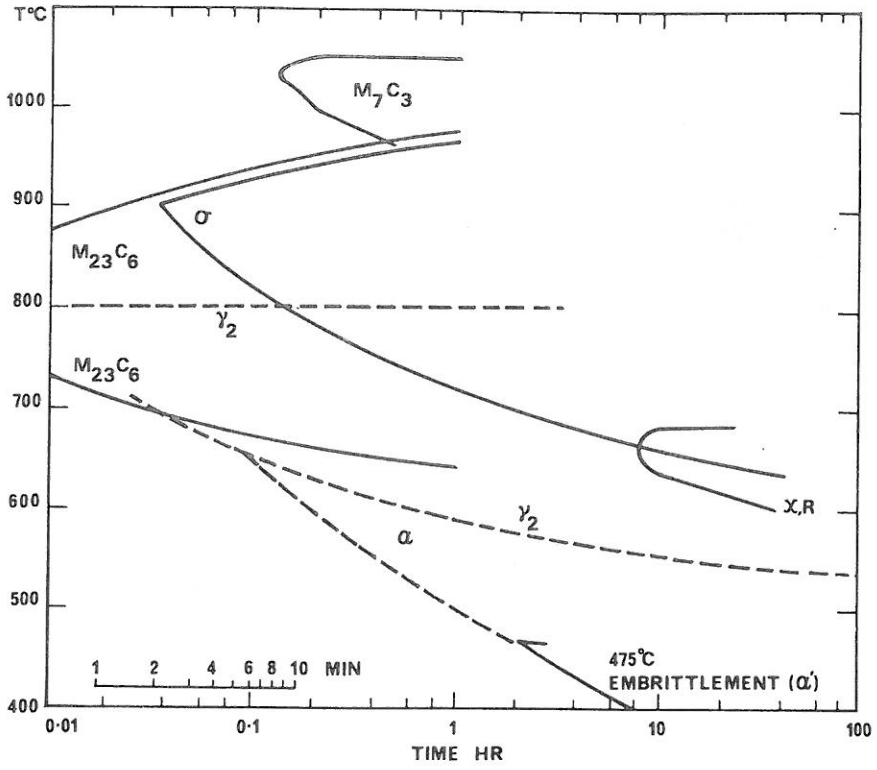

Fig. 4 T.T.T. diagram of a duplex U-50 alloy, after Solomon and Devine(6).

3.1 γ_2 - It is possible for austenite to precipitate inside the ferrite grains at lower temperatures independently of the precipitation of other phases. This type of austenite,

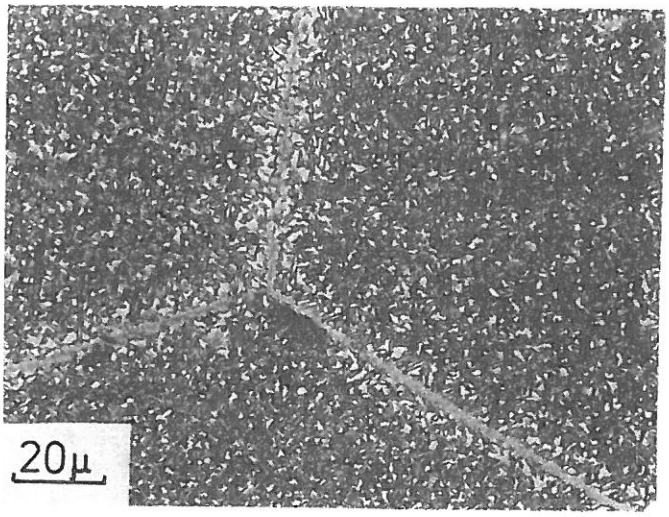

Fig. 5.
Fine precipitation of γ_2, formed after 20 hours at 600°C

Figure 5, designated γ_2 (6) is very fine and morphologically different from the high temperature austenite. At higher magnifications the γ_2 structure can be seen as a plate morphology occasionally twinned with a midrib separating the twinned regions, Figure 6. It is thought that this type of austenite precipitation is akin to the martensitic austenite referred to in a previous study (4), which is said to exhibit many characteristics of a shear transformation. A typical diffraction pattern and energy dispersive X-ray spectrum is also shown in Figure 6, and confirms the f.c.c. lattice structure. However, there is no significant difference in analysis between γ_2 and the parent ferrite matrix, which in itself suggests a diffusionless transformation.

3.2 $M_{23}C_6$ - The precipitation of $M_{23}C_6$ is very rapid and according to Solomon and Devine (6) requires less than one minute to nucleate at 800°C. In accordance with previous studies precipitation occurs in the regions depicted in the T.T.T. diagram in Figure 4. The austenite-ferrite boundaries are the most likely source of nucleation sites for $M_{23}C_6$ due to increased chromium level in the α and enrichment of carbon in the γ regions resulting from partitioning effects between phases. Several morphological variants of the precipitate have been observed including cuboidal and fibrous particles, and the occurence of a cellular precipitate type (7) has also been identified. Figure 7 shows an extraction replica of the cuboidal type particles which have precipitated at an interphase boundary. A typical energy dispersive spectrum is also shown, together with the elemental microanalysis which reveals a 60% Cr rich precipitate containing iron, molybdenum and manganese.

3.3 Sigma, σ - The body centered tetragonal sigma phase rich in chromium and iron is to be found in the temperature range 700-950°C, and formation can be as rapid as 15 minutes in a course grained casting at 900°C. Its presence in the duplex steel structure has the most deleterious effect of any phase on the impact properties of the alloys, and its formation should at all cost be avoided. The high chromium content in the σ phase leads to matrix depletion of this element and a subsequent reduction in corrosion performance. Sigma formation can be quite extensive in castings which are slow cooled in the mould, and Figure 8 shows partial transformation of ferrite to σ in an as-cast runner bar of three inches section thickness.

Figure 6 (a) Thin foil micrograph of γ_2 platelet, showing midrib between twinned regions. 20 hrs at 600°C.

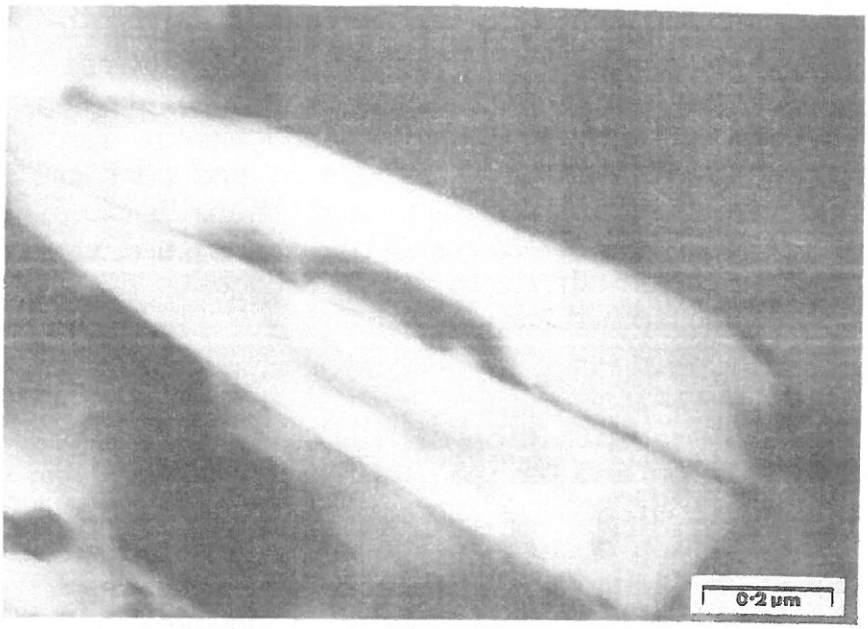

(b) Diffraction Pattern from above platelet confirming f.c.c. structure.

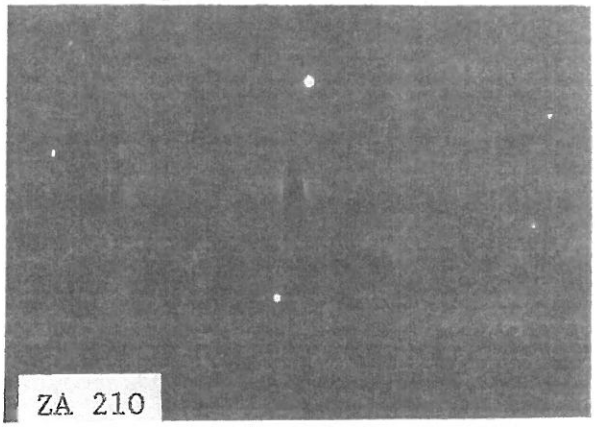

(c) Energy dispersive spectrum of γ_2, base ferrite composition.

Figure 7 (a) Extraction replica of cuboidal $M_{23}C_6$ precipitates. 5 Minutes at 800°C.

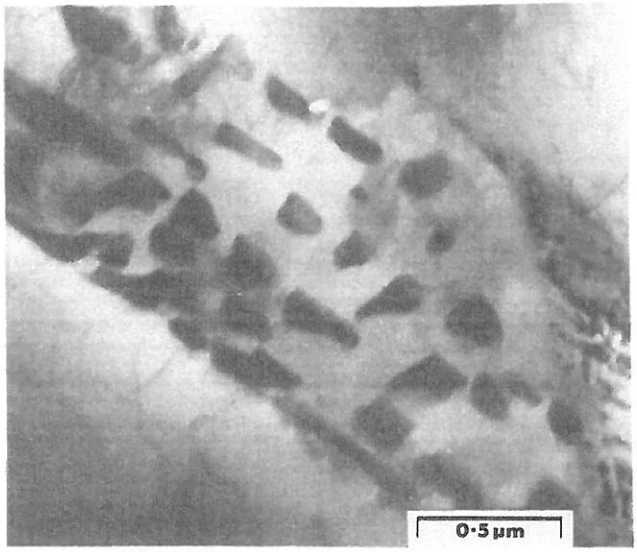

(b) Energy loss spectrum

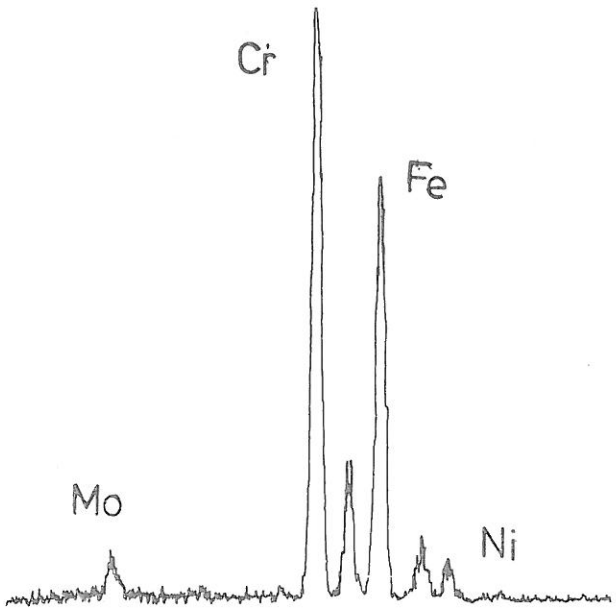

(c) Wt % Composition

Mo	Cr	Mn	Fe	Ni
11.96 ± 0.88	58.17 ± 1.36	4.56 ± 0.39	22.79 ± 0.89	2.52 ± 0.32

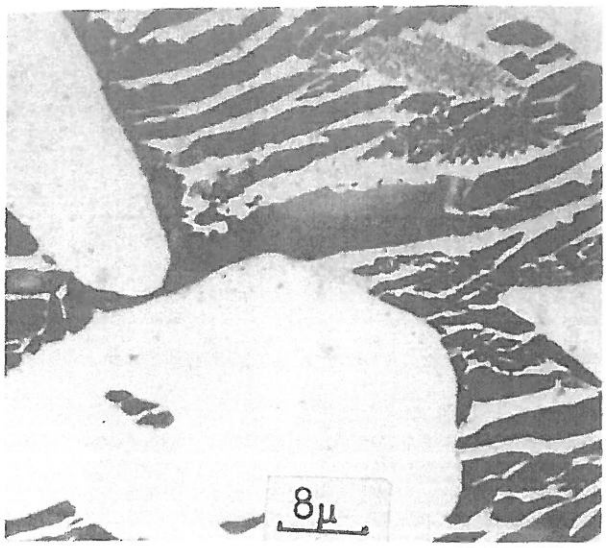

Fig. 8.
Transformation of α to a lamellar aggregate of σ and γ in a 3" section as-cast runner bar.

Its formation can be avoided by hot stripping from the mould and water cooling, but this procedure runs the risk of cracking on castings of varying section size.

As σ forms in the ferrite, the surrounding matrix is enriched in nickel and denuded of chromium. As a result a sympathetic nucleation of σ and γ occurs which gives rise to the lamellar structure shown in Figure 8. Various other feathery structures are also observed. Figure 9 is an extraction replica taken from a sample aged at 700°C for an hour and it reveals large plates of σ in close proximity to a finer precipitate discussed in the next section. A typical diffraction pattern and X-Ray spectrum analysis gives unambiguous phase identification.

3.4. 475°C Embrittlement - In the temperature range 450-525°C (higher upper limit temperatures are reported by other workers) an embrittling phenomenon is encountered in highly alloyed ferritic steels which seriously reduces the impact strength of the alloy. Literature pertaining to the identification of the actual precipitating phase appears confused. Although it has often been isolated and observed, its structure, composition and mechanism of formation is as yet not fully understood. It is designated α′ and believed to be either a high chromium containing solid solution (6,8) or a chromium nitride/carbonitride (9,10). Formation of α′ has been observed in two ways: nucleation and growth and spinodal decomposition. Spinodal decomposition, favoured by high chromium contents, has been most frequently reported (6,11). The reaction is reversible by reheating to a region of 600°C, whereupon the α′ dissolves.

Figure 9 (a) Extraction replica of sigma phase precipitation formed at 800°C after 1 hour.

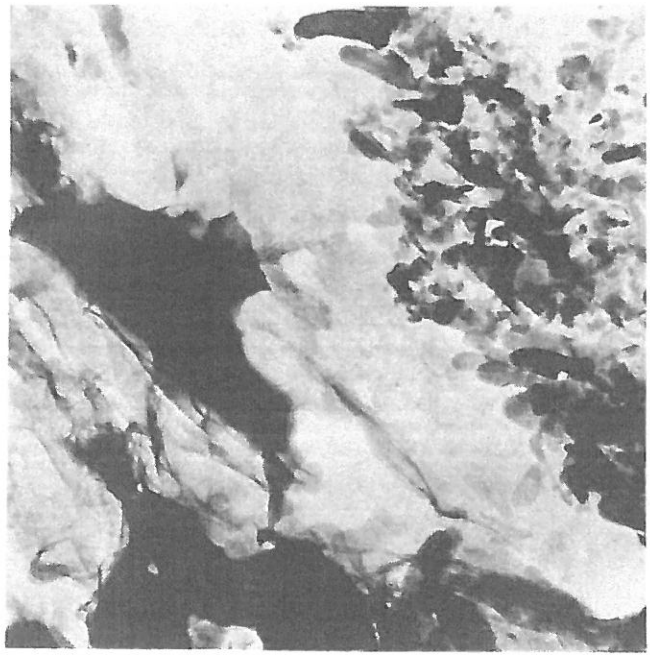

(b) Energy dispersive spectrum and diffraction pattern

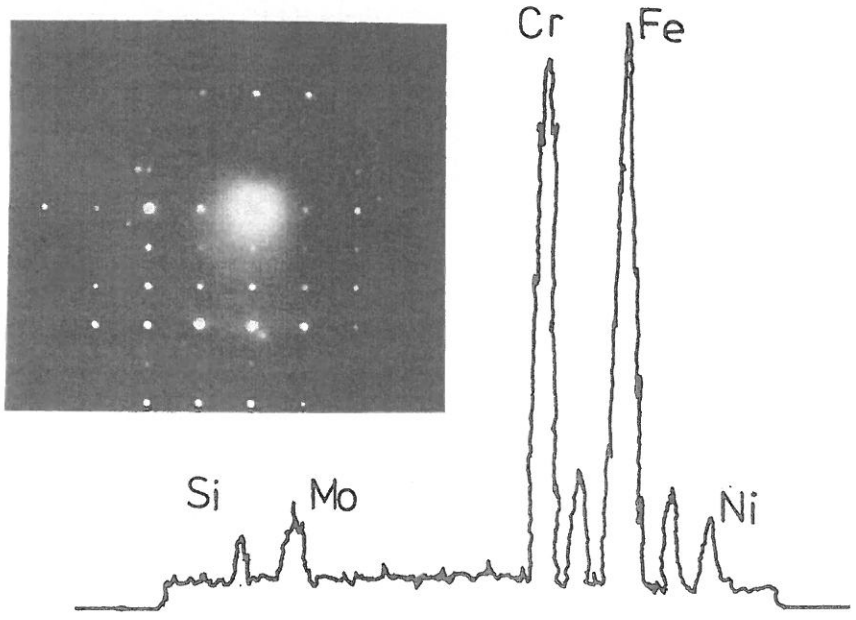

(c) Wt % Compositional Analysis.

Si	Mo	Cr	Mn	Fe	Ni
2.91	9.66	30.76	4.54	47.88	4.23

One fact is clear, α' is undetectable by light optical means and requires electron microscopy for accurate detection and analysis. However, specimens in this study isothermally transformed within this temperature range after ferritisation at 1310°C have produced a high proportion of optically visible precipitates in the ferrite.

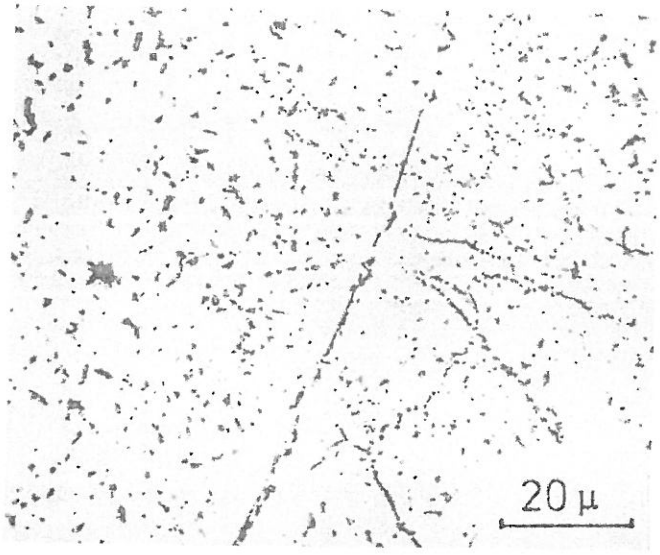

Fig. 10
Optical precipitates of possible carbide/ carbonitride type, after 5 hours at 500°C

Figure 10 for example shows precipitates at a grain boundary after transformation at 500°C for 5 hours. Embrittlement due to this visible precipitation occurs at much shorter times than the α' embrittlement predicted by Solomon and Devine (6), shown on the T.T.T. diagram of Figure 4. Precipitation of an hexagonal M_2X phase has also been observed and identified as such, but a stable phase boundary has yet to be established. Smith et al (12) have reported such a precipitate in a 25Cr-5Ni alloy, but at a much higher temperature of around 900°C. Figure 11 shows the needle like morphology of M_2X precipitates together with an X-Ray energy analysis. However, this optically visible precipitation may be associated with that occurring during the quench from the ferritising temperature already discussed, and may not be a true equilibrium phase normally associated with ageing in the 450°C - 525°C region. Work involving convergent beam electron diffraction continues in an attempt to resolve this question. It may be that this ultra-rapid precipitation sequence, controlled by nucleation and growth, has in previous investigations been confused with α' precipitation.

Evidence of α' precipitation can be seen in Figure 12 from a specimen aged at 475°C for 120 hours. The homogeneous dispersion of the precipitates in the ferrite grains appear to confirm previous work which suggests that the α'

Figure 11 (a) Replica of needle shaped M_2X precipitates in a specimen aged 2 hours at 650°C

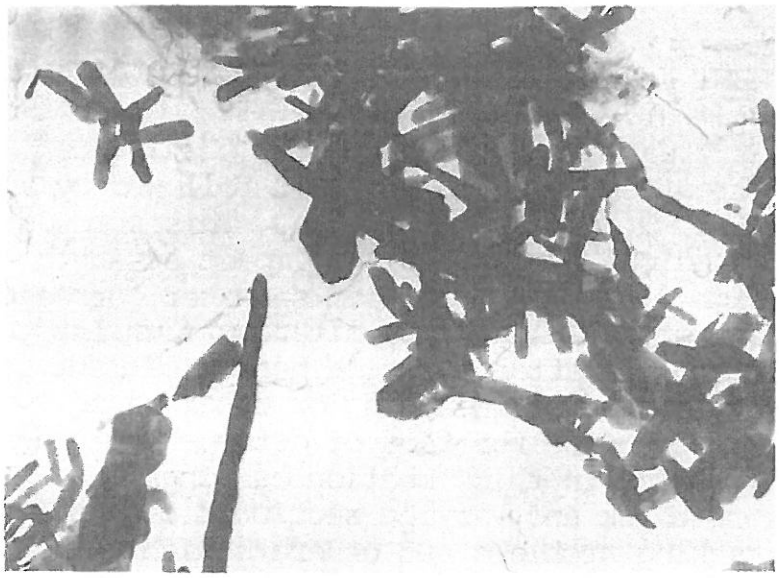

(b) X-ray energy analysis

	Wt % Composition			
Si	Mo	Cr	Mn	Ni
3.03 ± 0.63	14.81 ± 2.10	72.31 ± 3.25	3.74 ± 0.68	6.08 ± 0.92

Figure 12 (a) Fine matrix precipitation of α′ in a specimen aged at 475°C for 120 hours.

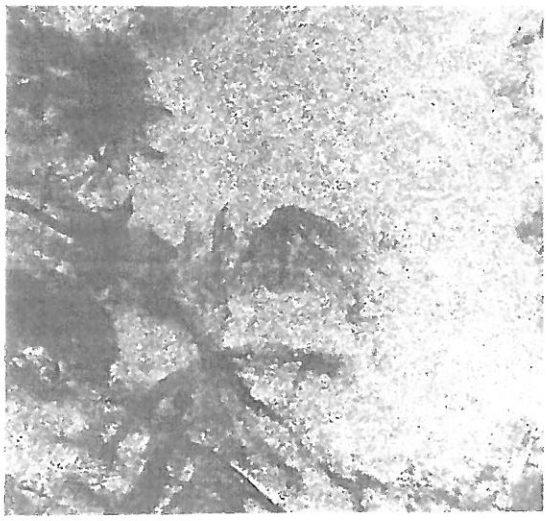

(b) Wt % Composition of α′

Si	2.98 ± 0.82
Mo	13.36 ± 2.52
Cr	64.89 ± 3.87
Mn	2.82 ± 0.74
Fe	13.58 ± 1.80
Ni	2.45 ± 0.71

precipitation is due to a spinodal mechanism. An energy dispersive spectrum is also shown in Figure 12, confirming a chromium rich phase, but diffraction work is continuing to confirm its crystallography.

4.0 HEAT TREATMENT

The standard heat treatment procedure after casting is a solution heat treatment at 1100 - 1120°C followed by a furnace cool to 1040°C and a water quench. This procedure gives optimum mechanical properties and impact strength coupled with a high degree of localised seawater corrosion resistance. Proprietry duplex alloy literature whilst recommending air cooling after solution heat treatment for thin sections, advises water quenching or other rapid cooling, and thus recognise the fact of detremental phase precipitation occurring in thick section castings. However, rapid quenching of thick and varying sectioned castings can cause serious cracking problems and generate high quenching stresses in excess of the yield stress. This problem is well known in the handling of the original duplex stainless steel, Cd4 M Cu. As manufacturers of large high pressure pumps, the section thicknesses of certain pump casing castings were approaching 8 to 10 inches. It was therefore a necessity to produce an alloy which was amenable to an air cool after solution heat treatment yet still retain excellent mechanical properties and corrosion resistance.

A series of alloys were cast with varying $\alpha\backslash\gamma$ ratios to study the effect of air cooling on 150mm diameter billets. Keeping to a nominal 25% Cr, 0.04%C, 0.1% N_2, 2% Mo composition, the α/γ ratio was adjusted by variations in the nickel content between 3 and 9%. Figure 13 shows the effect of $\alpha\backslash\gamma$ phase balance on mechanical properties at the centre of the billets after a solution heat treatment and water quench, whilst Figure 14, shows the variation of room temperature impact strength with the $\alpha\backslash\gamma$ ratio for different heat treatment states. The results in Figure 13 compare favourably with those of Floreen and Hayden (14) with respect to the rate of increase in yield strength and U.T.S. values with increasing ferrite content.

The results of Figure 14 contain the most important message.

At high ferrite contents the alloys behave in a brittle manner irrespective of heat treatment condition, due to the susceptibility of the ferritic matrix to cleavage fracture.

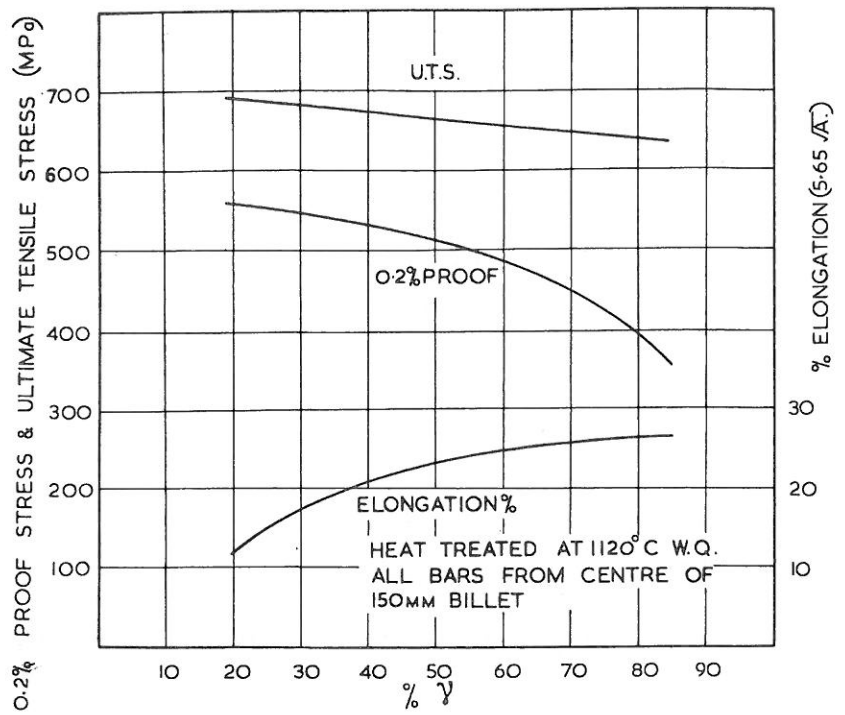

Fig. 13. The effect of α/γ phase balance on the room temperature thick section tensile properties.

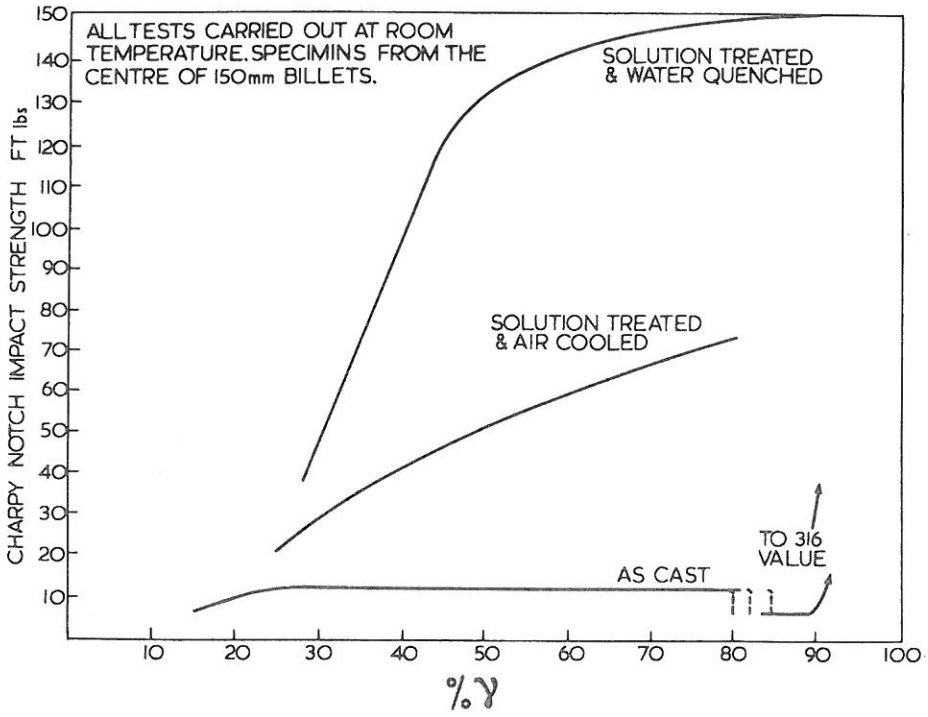

Fig. 14. The effect of α/γ phase balance on the room tensile, thick section, toughness properties.

It is this fact alone that is responsible for the instances of both quench cracking and cold cracking before "knockout" reported for those alloys with ferrite contents between 60 and 80% (e.g. Cd4 M Cu). Toughness in the air-cooled and water quenched conditions increases continuously with increasing austenite content, the water quenched toughness peaking at about 45% γ. In the as cast condition in thick section the toughness remains low whilst there is any ferrite in the microstructure due to precipitation of α' between 450 and 550°C.

The additional loss of impact strength in the as cast state at higher austenite contents results from σ formation in the ferrite. With increasing γ level there is an increasing tendency for chromium to partition to the ferrite and chromium levels of up to 33% have been measured by analytical electron microscopy. From previous work on sigma formation (15), the increased chromium levels in the ferrite massively accelerate its precipitation, and there is sufficient time on cooling in the mould at temperatures between 800-900°C for the ferrite phase to completely transform to a lamellar structure of sigma and austenite (as shown in Figure 8).

Considering these results together with computer calculated cooling curves for thicker sections, the $\alpha\backslash\gamma$ ratio for use in thick sections up to 200mm, which optimises mechanical properties and impact strength when air cooling is adopted, requires a minimum of 55% γ. The higher level of γ allows for the formation of cleaner microstructures obtained as a result of the higher solubility of γ for carbon and nitrogen, hence keeping precipitate particles to a minimum. This results in maintaining the excellent localised corrosion resistance of the alloy. There remains, however, the possibility of σ formation during cooling in the mould and it is necessary to solution heat treat after knockout before burning down of risers, etc., otherwise cracking problems will be encountered with propagation down the sigma network.

The results of this and other studies carried out has led us to adjust the composition of the alloy in production to give a minimum of 60% γ. Mechanical properties of a 70% γ alloy are somewhat lower than those shown in Table 2, but corrosion performance is virtually unaffected.

5.0 ALLOY DEVELOPMENT

It is clear from the above discussion that increasing the γ content of the alloy resulted in some sacrifice of proof stress. A strengthening through alloy addition was sought therefore to improve the stress level. Addition of the interstitial solid solution elements carbon and nitrogen is by far the most effective way of strengthening, through alloy addition, in both ferrite and austenite (16,17). Carbon is undesirable in stainless steels, which leaves nitrogen. Nitrogen is used extensively (up to 0.5%) in the austenitic stainless steels of the A.1.S.1.200 series, and results in imparting very high strength levels. However, the solubility of nitrogen in the duplex 25Cr 5Ni alloys reaches a maximum at approximately 0.2% (18). Severe gassing problems have been met in past experience when nitrogen levels of about this figure have been introduced to castings of the original base alloy composition.

It is well known that manganese additions in several ferrous and austenitic alloys are effective in promoting nitrogen solubility. In fact, the A.I.S.I.200 series alloys also contain manganese in levels of between 8 and 12%. (It was not for this reason that manganese was used in these alloys however. During the Korean war nickel was in short supply, so manganese was used as an alternative γ stabilising element and also to cheapen the alloys). However, manganese has been shown to adversely effect localised corrosion resistance in austenitic steels (19) and also to promote σ formation (20). It is clear also that increasing the γ content in the microstructure will increase nitrogen solubility, however, there is a net decrease in mechanical properties resulting from a loss of dispersion strengthening reflected in the sensitivity of the proof stress value with ferrite volume fraction at higher γ contents, Figure 13.

Our thesis was as follows:- there is evidence to show that manganese additions do not materially affect the phase balance (21). If a level of manganese addition could be found that aided nitrogen solubility without loss of toughness or corrosion performance, then improved mechanical properties should be achievable.

A series of alloys were cast with increasing manganese contents of approximately 1,3,5,8,10,12 and 15% using a base alloy of nominally 25% Cr - 6-7%Ni-2%Mo-0.05%N_2. A study was made of the effects on microstructure, tensile and hardness properties, and corrosion resistance was monitored

by cyclic anodic polarisation measurements. Nominal compositions and mechanical properties of the alloys are given in Table 3 below.

Table 3

Compositions of the manganese alloys used in the study; and mechanical properties.

Alloy	C	Cr	Ni	Mo	Mn	.2%P.S.(MPa)	U.T.S.	Elong
1.	0.046	25.06	5.48	3.46	1.61	437	672	29
2.	0.049	25.43	5.17	2.69	3.87	481	695	29
3.	0.051	24.83	5.76	2.60	5.08	450	680	36
4.	0.043	24.37	7.31	2.29	8.39	462	672	37
5.	0.041	23.42	7.12	2.48	12.04	440	670	35

The effect on microstructure was surprising. Manganese is often categorised as a γ stabiliser and as such should be expected to increase the γ content of the alloy with increasing concentration. This was not the case, and up to 8% Mn had little effect on the volume fraction of γ. This was in agreement with previous work (21) which found manganese to behave more like that of a ferrite stabiliser when present in levels greater than 5%. Proof stress and U.T.S. values are fairly constant, while there is a progressive increase in hardness at manganese contents of 5% and more which is attributable to formation of σ and other precipitates in the microstructure. Ageing treatments in the temperature range 750-950°C followed by impact testing and metallography have confirmed the fact that manganese promotes the rate of sigma formation. This is shown in Figure 15, together with results from previous studies. It also appears that manganese increases the temperature range over which σ formation can be expected. A simulated cooling curve for a 150mm diameter air cooled ingot is also added, to show that this section size can be successfully air cooled from solution heat treatment without risk of σ formation.

Corrosion resistance was qualitatively assessed using critical pitting and crevicing temperatures as criteria (22). Anodic polarisation measurements in artificial seawater solution were made using sweep rates of 80 mV per minute. The variation of the critical corrosion temperatures with manganese content is shown in Figure 16. It can be seen that after 3% Mn, the critical pitting temperature is markedly decreased, while 3 to 4% Mn increases the critical crevicing temperature slightly, after which there is progressive deterioration.

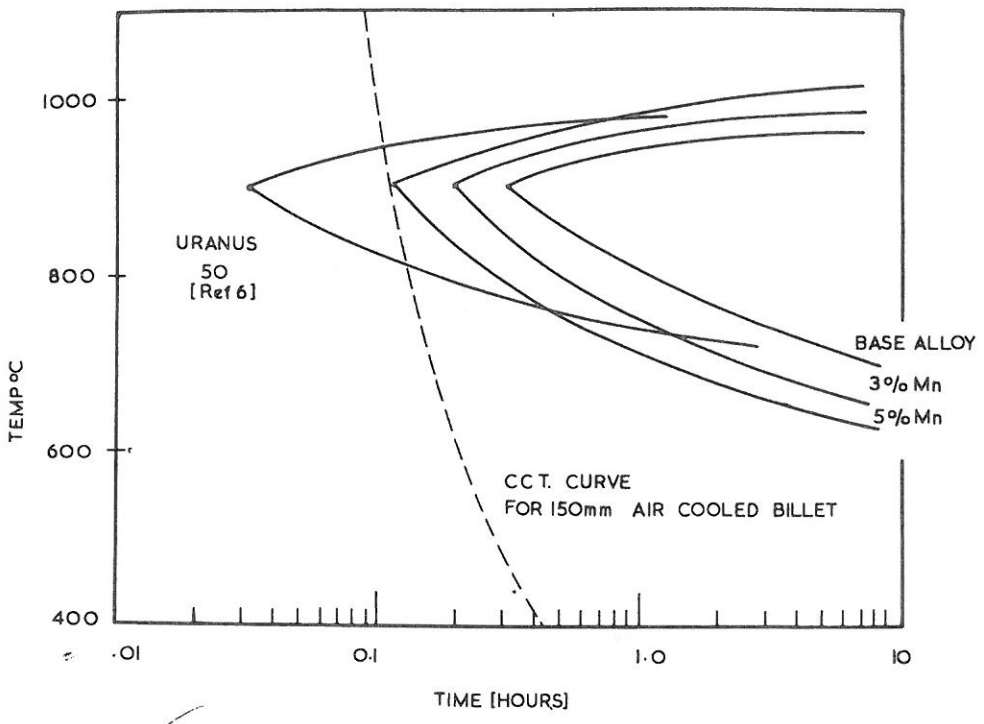

Fig. 15. Rate of formation of sigma in a series of alloys containing manganese additions.

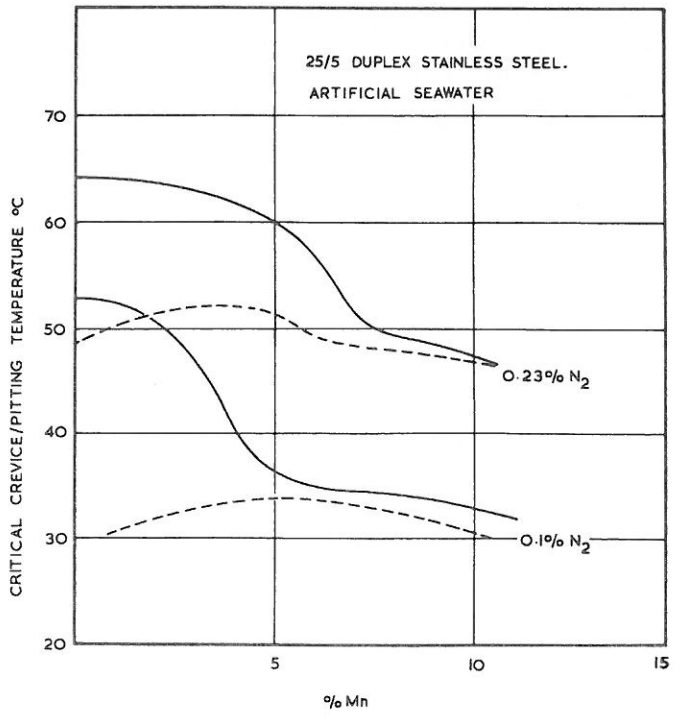

Fig. 16. Variation in critical pitting and crevicing temperatures with manganese for two nitrogen levels.

Considering the above results it was decided to adopt a manganese level of 4 to 5%. To examine the effect of this level of manganese on the nitrogen solubility, several alloys were cast with nitrogen contents varying from 0.05 to 0.35% in two series of alloys, the base duplex alloy and one containing the optimised manganese content. The test blocks were examined for degree of gassing both internally and externally, and it was clear that the alloys without manganese had gassed severely above 0.15%N, whereas the manganese containing alloys showed good soundness up to 0.3%N.

Nitrogen being a very strong austenitiser however increased the γ content of the alloys with increasing addition. At 0.35%N austenite became the continuous phase, consuming 90-95% of the microstructure, Figure 17.

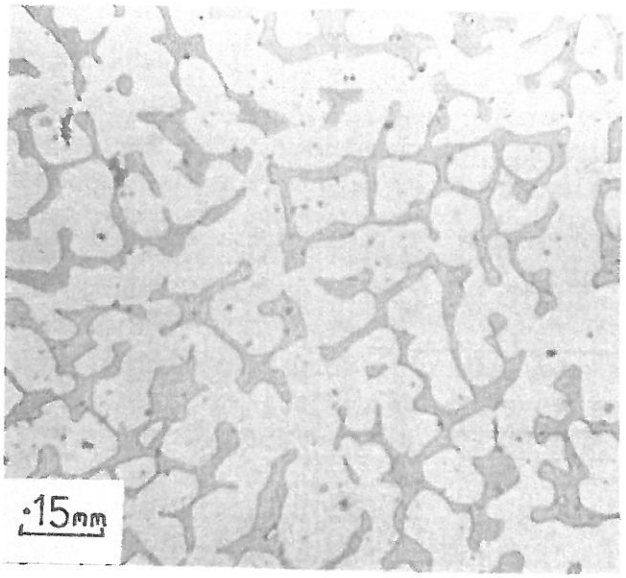

Fig. 17. Microstructure of a manganese/nitrogen alloyed steel with .35% N.

The dendritic appearance of the austenite suggests that austenite may have been the first phase to solidify. Further melts were therefore carried out to establish an optimum nickel-nitrogen balance which would enable an alloy of 70-75% γ to retain between 0.25 and 0.3%N.

A typical composition of the finalised alloy is shown below in Table 4, together with increased mechanical properties.

Table 4

Typical Composition and mechanical properties of the nitrogen strengthened alloy.

C	Cr	Ni	Mn	Mo	N	.2% P.S.	U.T.S.	Elong %
.04	24	6	4.5	2.2	.25	540	720	38

This alloy is designated Zeron 26 (b)

6.0 CORROSION STUDIES

Previous work has shown that nitrogen is beneficial in aiding localised corrosion resistance (23), and is also shown to have a linear relationship with the critical pitting temperature in 316 type alloys (19). Earlier work with the standard duplex alloy had also shown increased critical crevicing and pitting temperatures due to nitrogen in the series of manganese containing alloys. Figure 16.

A series of alloys of the 65-75% γ family with varying nitrogen contents of between 0.05 and 0.35% were evaluated to determine the precise effect of the nitrogen addition. Using a cyclic anodic polarisation method, the critical pitting and crevicing temperatures were determined and are shown in Figure 18.

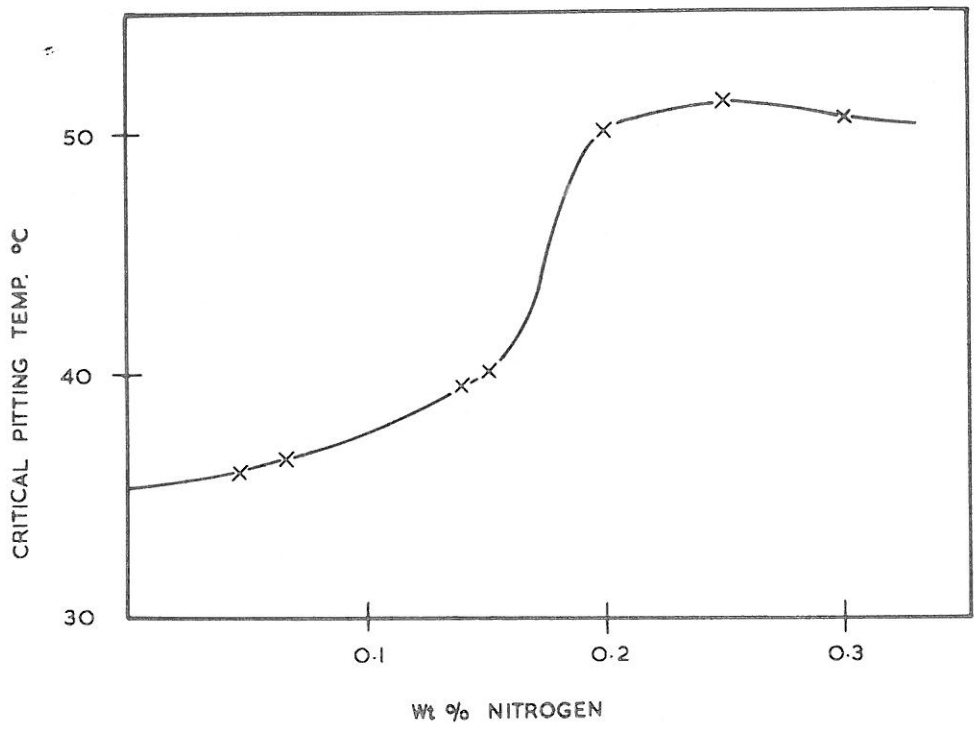

Fig. 18. Critical pitting temperatures for a family of nitrogen containing alloys.

(b) Zeron 26, patent applied for, is a Registered Trade Mark of Mather & Platt Ltd.

The results show a steady increase in corrosion resistance up to a saturation level of just over 0.2%N. Thus a minimum of 0.2% nitrogen is required in the new improved alloy for increased corrosion resistance, and further additions are effective only in increasing mechanical properties (24).

The alloy is well capable of handling sour well waters, and Figure 19 is a comparison of critical pitting and crevicing temperatures between the new manganese/nitrogen alloy, and a modified 5% Mo bearing CN7M austenitic alloy.

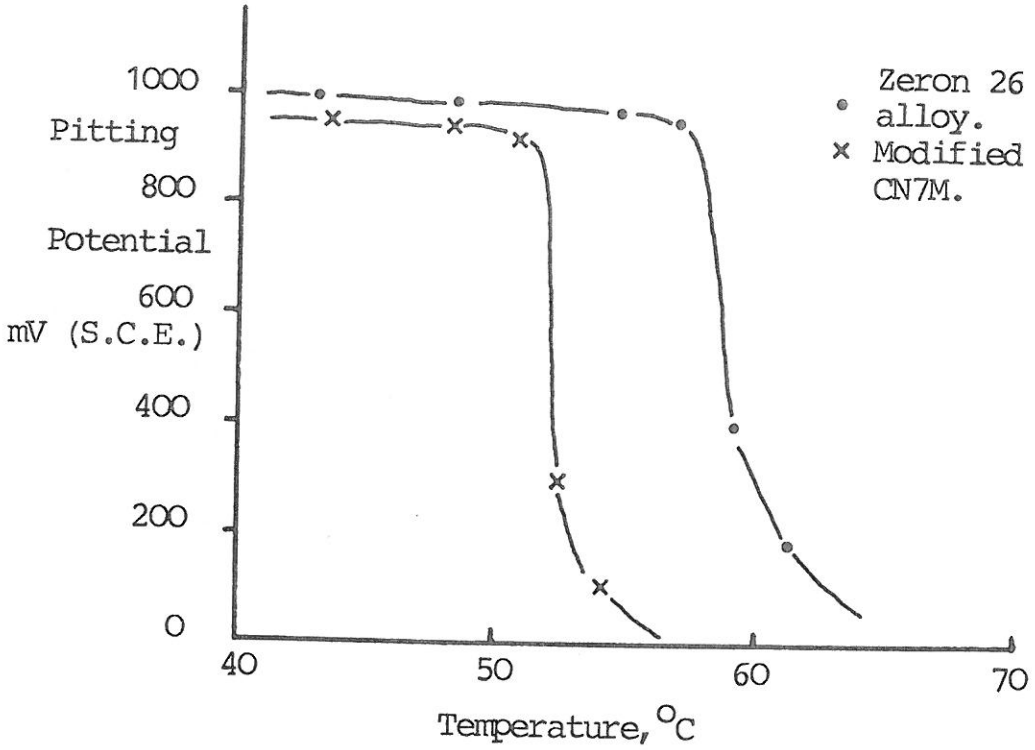

Fig. 19. Comparative critical pitting temperatures of Zeron 26 and a modified CN7M alloy, in a sour well water.

Water Composition

pH 4.2., Cl- 136,000 mg/L,
H_2S 6 mg/L, TDS 222,000 mg/L,
CO_2 300 mg/L, $O_2 < 5$ p.p.b.

Critical Crevicing Temperatures, ^{o}C

Zeron 26	50
Modified CN7M	39
CF8M (316)	20

As can be seen the critical pitting temperature is well in excess of the higher molybdenum alloy and the manganese containing duplex alloy has a superior critical crevicing temperature. The general corrosion resistance of the two alloys is comparable in these waters when measured by means of linear polarisation (25).

General Corrosion Rate in the sample sour well water,

Zeron 26	0.43×10^{-3} mm per year
Modified CN7M	0.50×10^{-3} mm per year

7.0 WELDING

Welding of the base 25Cr7Ni-2Mo alloy has always been successful using a specially prepared matching manual metal arc rod. These rods have always contained a higher percentage of nickel than the base alloy, and therefore deposit a microstructure high in austenite.

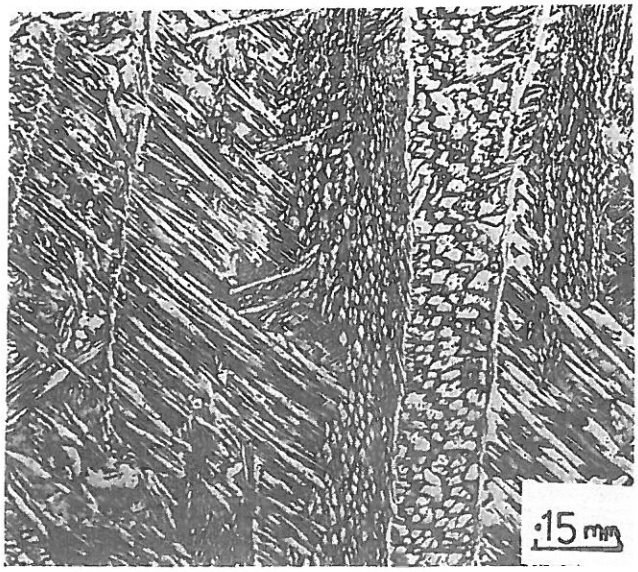

Fig. 20. As deposited weld metal microstructure

As deposited, as well as solution heat treated weld metal has always possessed high ductility and toughness with more than matching tensile properties. Table 5 shows values obtained from a weld pad build up in a base material plate.

Table 5

Composition and room temperature mechanical and impact properties of matching S.M.A.W. weld deposit.

C	Mn	Cr	Ni	Mo	N
.03	1.33	25.53	7.14	2.32	.10

	.2% P.S. MPa	U.T.S. MPa	Elong %	Impact. J
As welded	750	803	20	45
Soln. ht. trt. 1100°C air cool.	620	750	34	96 (Charpy-V)

The as welded H.A.Z. does show a very narrow austenite free ferrite zone along the fusion boundary on the parent metal side, which can give rise to some lack of ductility in side, root and face bend tests, and cracking has been noticed in as welded test pieces. Test procedures carried out on 76mm 3" thick double-V-butt welded plates do prove excellent radiographic standard welds with adequate through thickness ductility. Moderate nitrogen levels in the weld metal of approximately 0.2% promote rapid formation of austenite from ferrite as the weld metal cools and thus increases ductility and helps avoid weld metal cracking. The duplex austenitic ferritic structure also avoids any tendency for solidification cracking and micro-fissuring in the austenite.

In carrying out heavy weld reapir, or even heavy machining it is advantageous to carry out a stress relieving heat treatment, although with the move to an air cooling alloy this is somewhat less of a problem. However, as shown in the section on a microstructure, the number of embrittling phases present in the alloy system makes stress relieval of a duplex steel almost impossible without risk of severe embrittlement. A maximum temperature of 350°C is insufficient to generate effective thermal jogging to relieve a high stressed component.

Consideration of Figure 4, however, shows that if a duplex steel were heated to a temperature of 570° + 20°C, for a period of up to eight hours and a subsequent air cool through the 425-500°C region of α' precipitation, stress relief

should be achieved without significant loss of impact strength. Experience has shown this to be the case, and the duplex alloy Zeron 25 exhibits impact values of 80 and 110 Joules after heat treatment for 6 hours at 570°C in the forged and cast conditions respectively. Solomon and Devine (6) have carried out exhaustive tests to check the effect of ageing at temperatures of 600°C on localised properties, and have reported no deliterious effects. Direct measurements of internal stresses using the strain gauge stress relaxation technique has shown surface internal stresses to have been reduced from the yield stress (compressive) after quenching, to less than 5% of this value after heat treatment at 560°C.

A study has been made of the C.T.O.D. values of the 65-75% austenite alloy welded in 35mm sections, measurements being made in the centre of the weld, and down the H.A.Z. in specially designed specimens to check the ductility of the welds before and after heat treatment. The consumables used were a matching filler and one of a 318 type alloy containing nominally 19%Cr, 12%Ni, 3%Mo. These results are presented in Table 6.

Table 6

C.O.D. δ_c values for weld metal and H.A.Z. in a 25Cr-7Ni-2Mo 32mm butt welded plate.

	As Welded δ_c (mm)	Soln. Ht.Trt.	570°C-4 Hrs.
Weld:-	0.27	0.85	0.30
	0.44	1.08	0.25
H.A.Z.:-	.32	1.38	0.21
	.34	1.01	0.20

It is clear that even in the as welded state the H.A.Z. specimens show good toughness levels, improving to a very high value after solution heat treatment. However, the specimens treated for 5 hours at 570° have suffered embrittlement, but still retain an acceptable C.T.O.D. value, and are without internal welding stresses. Values of the weld metal C.T.O.D. compare closely to those obtained in recent work carried out at the British Welding Institute (26).

SUMMARY

In order to extract the best performance from the duplex alloys the role and relative importance of the alloy additions must be fully appreciated. The importance of the austenite-ferrite phase balance cannot be overstressed. High ferrite contents should be avoided since they can lead to susceptibility to quench cracking and poor air cooled thick section toughness.

To produce thick section castings the alloy must be air cooled from solution heat treatment temperatures to avoid possible quench cracking and high internal stresses. This is possible only by controlling the major alloying elements to produce higher austenite (65-75%) content alloys.

An intermediate stress relieving temperature has been shown to be available to minimise welding stresses and internal stresses which give rise to dimensional instability problems.

Localised corrosion resistance is increased significantly by the addition of nitrogen to a 0.2% minimum level. The increased solubility of nitrogen by the addition of manganese increases proof stress values by up to 100 MPa.

Increasing manganese contents increase the rate and temperature of formation of sigma phase.

REFERENCES

1. J.E. Truman, Stainless Steel Industry, Vol. 7, No. 39. Sept. 1979 p. 15

2. J.E. Truman, Metallurgist and Materials Technologist, Vol. 12. Feb. 1980 p.75

3. M.J. Mathews, Metallurgist and Materials Technologist, Vol. 14. No. 5. May 1982 p.205

4. P.D. Southwick and R.W.K. Honeycombe, Met. Science. July 1980. Vol. 14, No. 7 p.253.

5. J. Hochmann, A. Desestret, P. Jolly and R. Mayoud, Metaux Corros. Ind. Parts I, II and III Nov., Dec. 1974. Vol.50, and Jan 1975 Vol. 51.

6. H.D. Solomon and T.M. Devine, Optimisation of processing Properties and Service Performance through Microstructural Control, MiCon'78.

A.S.T.M. STP672 1979pp. 430-461

Editors. Abrams, Maniar, Nail and Solomon.

7. F.R. Beckitt, J. Iron Steel Inst. 1969, Vol. 207. p.632.

8. R.M. Fisher, E.J. Dulis and K.G. Caroll, Trans. A.I.M.E. 1953, 197. p.690.

9. A. Plumtree and R. Gullberg, Metall. Trans. A.7A Sept. 1976.

10. A. Hendry, Z.F. Mazur and K.H. Jack, Metal Science Aug. 1979, p.482.

11. R. Lagneborg, A.S.M. Trans. Quart., 60, 1967. p.17.

12. C.J.E. Smith, J.C. Ruckman and G.D. Lawrence, Metals and Materials. May 1973, P.234.

13. U.S. Patent, 3,065, 119 November 20, 1962.

14. S. Floreen and H.W. Hayden, Trans. A.S.M. 1968, Vol. 61, p.489.

15. F.J. Shortsleeve and M.E. Nicholson, Trans. A.S.M. 1951, Vol. 43. p.142.

16. K.J. Irvine, D.T. Llewellyn and F.B. Pickering, J. Iron Steel Inst. 1961, Vol. 199, p.153.

17. K.J. Irvine and F.B. Pickering, ibid 1963, Vol. 201. p.944.

18. J.F. Elliot, M. Gleiser and V. Ramakrishna,'Thermochemistry for Steelmaking' Vol. II. Adison and Wesley Publishers. 1963.

19. R.J. Brigham and E.W. Tozer, Corrosion, N.A.C.E., Vol. 30. No. 5, May 1974. p.161.

20. F.B. Pickering, Sheffield Polytechnic, Private Communication.

21. P. Guiraldenq, Memoires Scientifiques Rev. Metall. LXlV, No. 11, 1967, p.907.

22. N.D. Greene, Corrosion, N.A.C.E. Vol. 18. Ap. 1962. p.136.

23. W.H. Richardson and P. Guha, B. Corros. J. Vol. 14. No. 3, 1979, p.167.

24. J. Hochmann, 'Materiaux et Techniques', Special Issue on Manganese, December 1977, p.69.

25. M. Stern and A.L. Geary, J. Electrochem. Soc. Vol. 104, No. 1, Jan. 1957, p.56.

26. J. Honeycombe and T.G. Gooch, Welding Institute Research Report No. 42/1977/M. June, 1977.